

# **Supplementary Information**

## **A glutamine amide flip elicits long distance allosteric responses in the LOV protein Vivid**

Abir Ganguly<sup>1</sup>, Walter Thiel<sup>1</sup> and Brian R. Crane<sup>2\*</sup>

\*Author to whom correspondence should be addressed [bc69@cornell.edu](mailto:bc69@cornell.edu)

1. Max-Planck-Institut für Kohlenforschung, Kaiser-Wilhelm-Platz 1. 45470 Mülheim an der Ruhr, Germany
2. Department of Chemistry and Chemical Biology, Cornell University, Ithaca, New York 14853, USA

### **Contents**

1. Supplementary Figure S1: RMSDs of Gln182 with respect to the crystal structure in various VVD states during MD simulations.
2. Supplementary Figure S2: Hydrogen bonding pattern in the active site of the LOV domain in various VVD states during MD simulations.
3. Supplementary Figure S3-S4: Conformation of Gln182 in various VVD states obtained from REMD simulations.
4. Supplementary Figure S5: Dynamics of the N-terminal latch in various VVD states obtained from REMD simulations.
5. Supplementary Figure S6: DCCMs of VVD in various states constructed from MD simulations.
6. Supplementary Figure S7: DCCMs of VVD in various states constructed from REMD simulations.
7. Table S1: Correlations of hinge-ββ residues to the N-terminal latch.
8. Supplementary Figure S8: Convergence of the string simulations.
9. Force field parameters of flavin in various states.

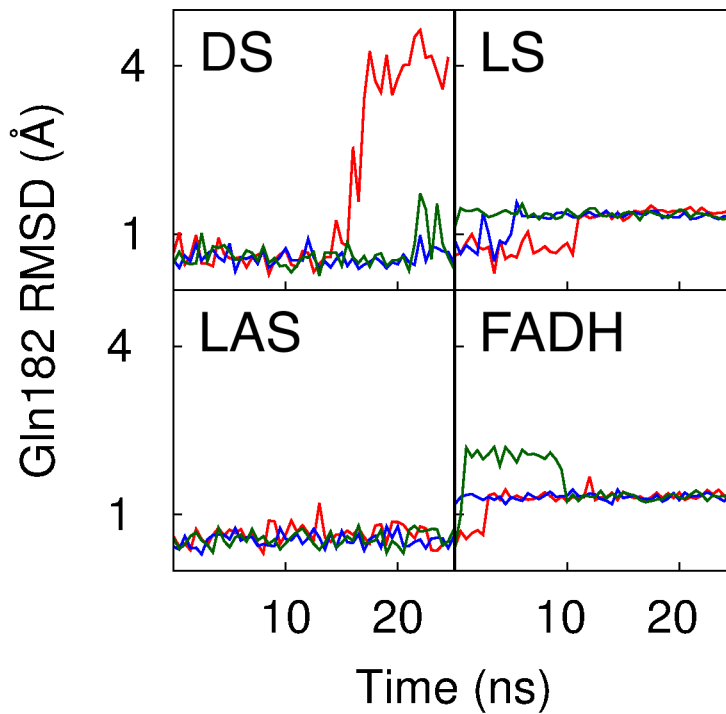


Figure S1. RMSDs of Gln182 with respect to the crystal structure in various VVD states during MD simulations. Plots are shown for DS, LS, LAS, and FADH, with red, blue, and green lines corresponding to independent MD trajectories. In DS, the RMSD fluctuates but remains less than 1 Å for major parts of the MD simulations indicating that Gln182 is somewhat flexible but remains mostly close to the crystal conformation facing FAD with its amide; in the later stage of one trajectory (red) the Gln182 rotates out of the active site away from the FAD. In LS and FADH the RMSDs stabilizes at a value slightly greater than 1 Å, in a conformation in which the residue faces FAD with its carbonyl. In LAS, Gln182 faces FAD with its carbonyl already in the crystal structure, and the RMSD remains close to zero suggesting that in this state the Gln182 is stable in the crystal conformation.

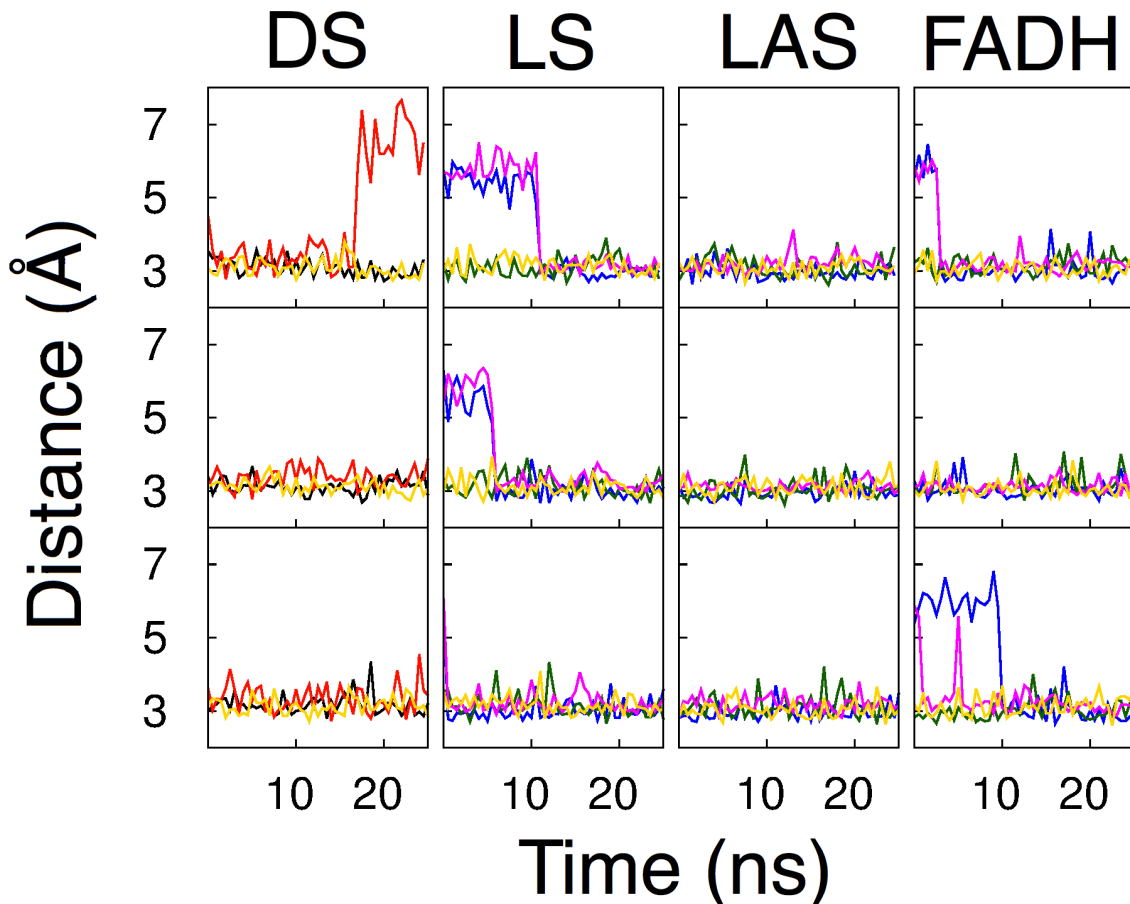


Figure S2. Hydrogen bonding pattern in the active site of the LOV domain in various VVD states during MD simulations. Key hydrogen bonding interactions of the active site are illustrated for VVD in DS, LS, LAS, and FADH (columns 1-4). The three rows refer to three independent MD trajectories. The following hydrogen bond distances are plotted: for DS, NE2(Gln182)-O4(FAD) (red), N(Gln182)-O(Ala72) (black), and N(Asn161)-O4(FAD) (gold); for LS, LAS, and FADH, OE1(Gln182)-N5(FAD) (purple), NE2(Gln182)-O(Ala72) (blue), N(Gln182)-O(Ala72) (green), and N(Asn161)-O4(FAD) (gold). The following hydrogen bonds are stable during the MD simulations: in DS, N(Gln182)-O(Ala72) (black) and N(Asn161)-O4(FAD) (gold); in LS, LAS, and FADH, OE1(Gln182)-N5(FAD) (purple), NE2(Gln182)-O(Ala72) (blue), and N(Gln182)-O(Ala72) (green). Note that in one trajectory of FADH, the Gln182 transition occurs within the equilibration stage of the simulation.

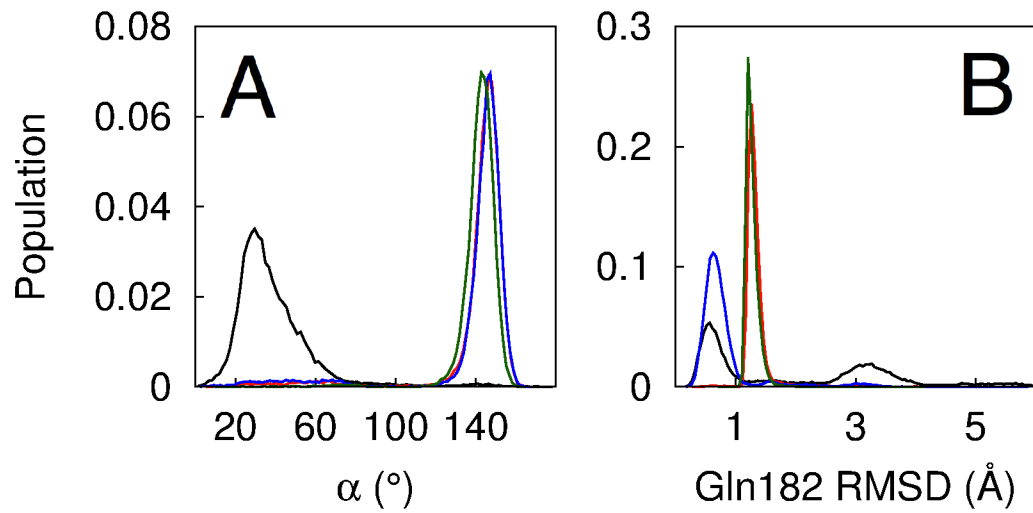


Figure S3. Conformation of Gln182 in various VVD states obtained from REMD simulations. (A) Distribution of angle  $\alpha$  (defined in Figure 2A of the main paper) in DS (black), LS (red), LAS (blue), and FADH (green). (B) Distribution of RMSDs of Gln182 in DS (black), LS (red), LAS (blue), and FADH (green). In DS, Gln182 is flexible but mostly faces FAD with its amine and remains close to its crystal conformation as indicated by a broad distribution of  $\alpha$  centered around 30° (A, black) and a small RMSD peak at less than 1 Å (B, black) (see Figure 2H of the main paper); a second smaller RMSD peak at ~ 3 Å represents configurations in which Gln182 rotates out of the active site (see Figure 2G of the main paper). In LS and FADH, Gln182 predominantly faces FAD with its carbonyl and mostly remains in this conformation as illustrated by a sharp  $\alpha$  peak at ~ 150° (A, red, green) and a single sharp RMSD peak at values slightly higher than 1 Å (B, red, green). In LAS, Gln182 also predominantly faces FAD with its carbonyl (sharp  $\alpha$  peak at ~ 150°; A, blue) but is somewhat more flexible than in LS and FADH as suggested by a comparatively low RMSD peak at less than 1 Å (B, blue).

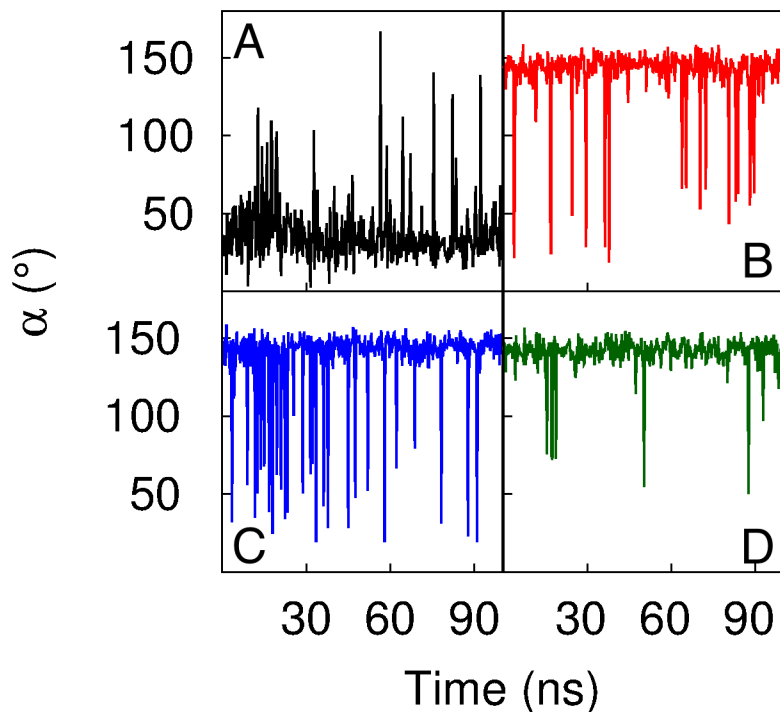


Figure S4. Conformation of Gln182 in various VVD states obtained from REMD simulations. Angle  $\alpha$  (defined in Figure 2A of the main paper) is plotted for the lowest temperature ensemble of the REMD simulations for DS (black), LS (red), LAS (blue), and FADH (green). In each case, the peaks correspond to transitions of Gln182 between two conformations: facing FAD with its amine ( $\alpha \sim 50^\circ$ ) and facing FAD with its carbonyl ( $\alpha \sim 150^\circ$ ).

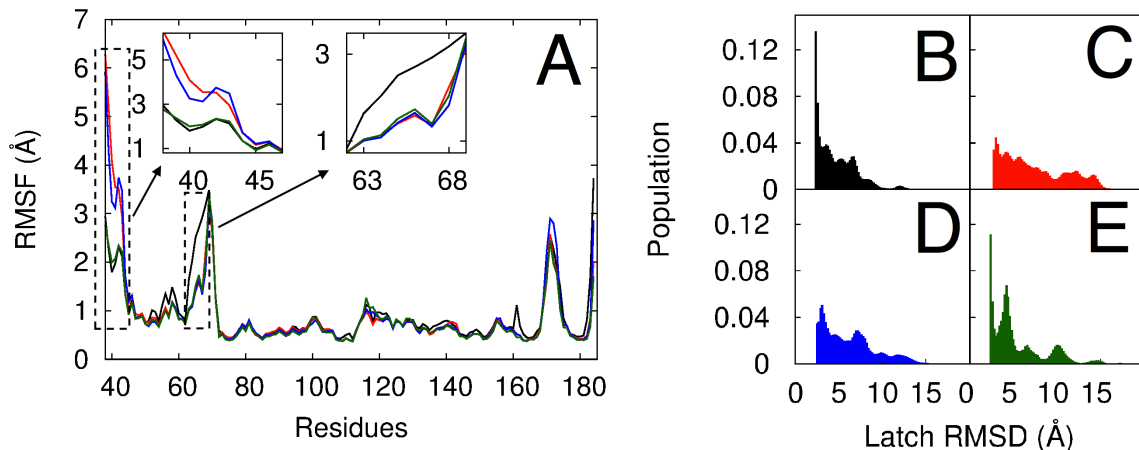


Figure S5. Dynamics of the N-terminal latch in various VVD states obtained from REMD simulations. (A) RMSFs of residues in DS (black), LS (red), LAS (blue), and FADH (green); those of residues in the N-terminal latch (residues 38-45) and the  $\beta\beta$  region (residues 62-69) are highlighted in the insets. (B-E) Distribution of RMSDs of the N-terminal latch with respect to the crystal conformation in DS (B), LS (C), LAS (D), and FADH (E). In DS, VVD has low latch flexibility and high  $\beta\beta$  flexibility as indicated by the RMSFs of the corresponding regions (A, black); the rigidity of the latch in DS is reflected in the latch RMSD distribution (B) that exhibits a sharp peak close to 3 Å and a negligible population beyond 10 Å. In LS and LAS, VVD has high latch flexibility and low  $\beta\beta$  flexibility (A, red, blue); the corresponding latch RMSD distribution has significant population (beyond 10 Å) of configurations in which the latch has been released. In FADH, both the latch and the  $\beta\beta$  region have low flexibility (A, green); however, in the corresponding latch RMSD distribution, there is a significant population of configurations with the latch released (E).

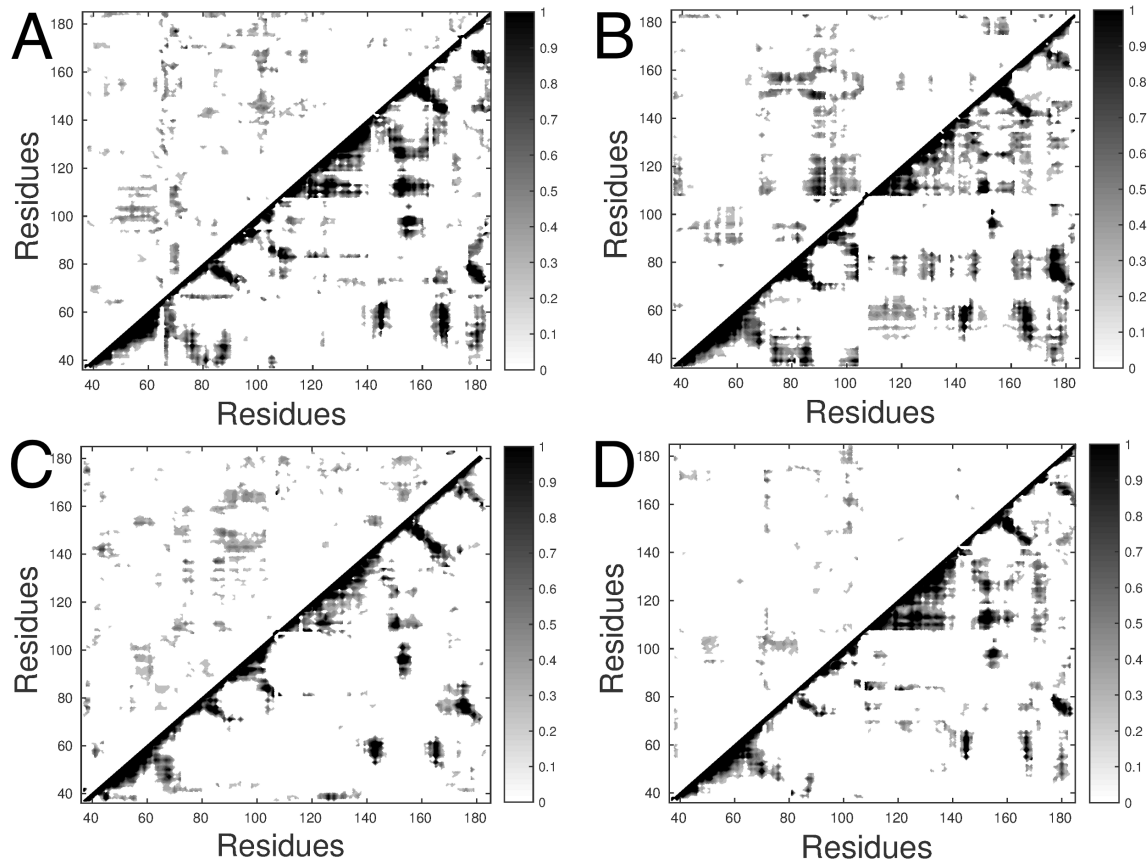


Figure S6. Correlated motions in VVD. DCCMs are constructed from MD simulations for VVD in DS (A), LS (B), LAS (C), FADH (D). In each case, the DCCMs are obtained from a single trajectory obtained by concatenating the various independent trajectories for that case. DCCMs obtained from individual MD trajectories were qualitatively similar. The upper triangle corresponds to positive correlations and the lower triangle corresponds to negative correlations.

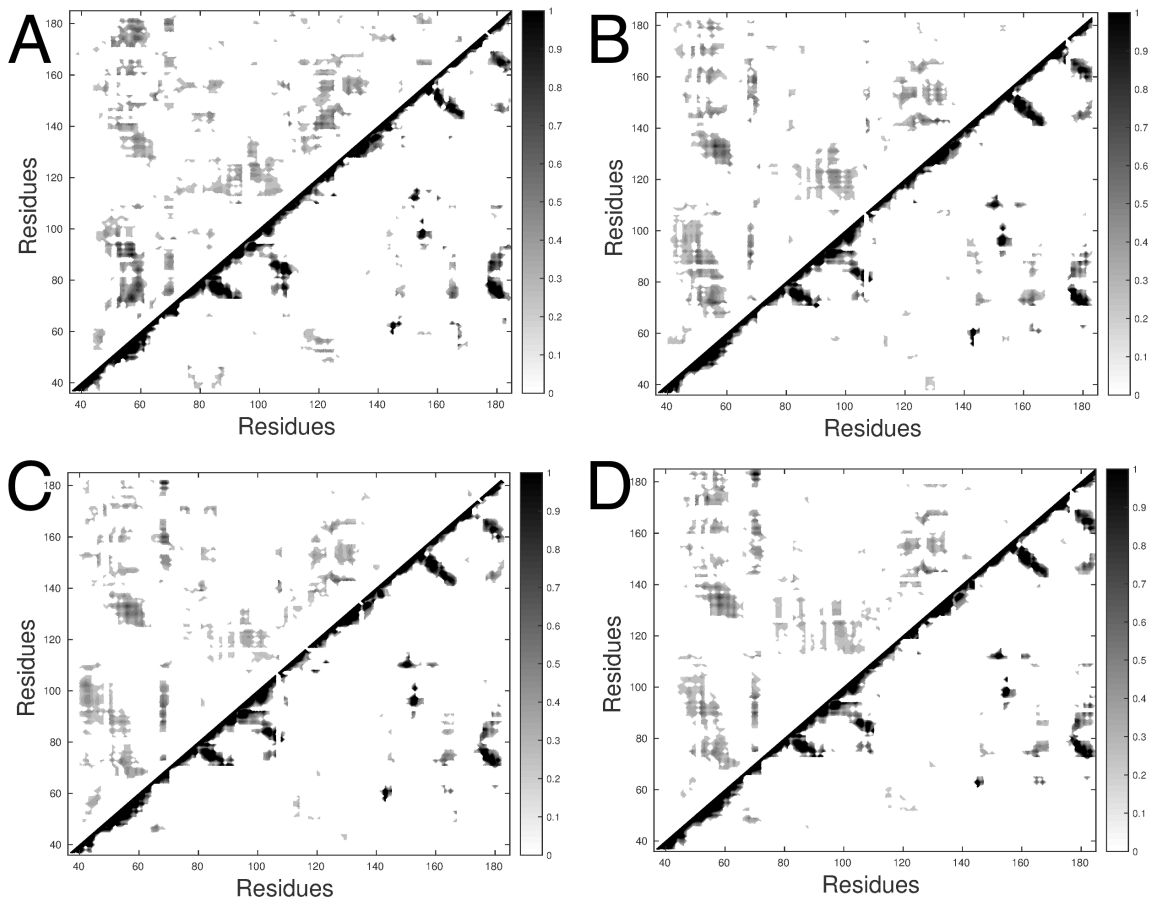


Figure S7. Correlated motions in VVD. DCCMS are constructed from REMD simulations for VVD in DS (A), LS (B), LAS (C), FADH (D). The upper triangle corresponds to positive correlations and the lower triangle corresponds to negative correlations.

Hinge- $\beta\beta$ residues	DS		LS		LAS		FADH	
	MD	REMD	MD	REMD	MD	REMD	MD	REMD
62	0.19	0.26	0.03	0.31	0.06	0.36	0.11	0.25
63	0.27	0.24	0.00	0.24	0.00	0.32	0.12	0.21
64	0.10	0.18	0.00	0.24	0.05	0.35	0.17	0.21
65	0.0	0.09	0.00	0.28	0.17	0.35	0.10	0.16
66	0.02	0.13	0.00	0.29	0.20	0.41	0.25	0.18
67	0.13	0.15	0.00	0.25	0.16	0.33	0.20	0.20
68	0.04	0.06	0.00	0.31	0.26	0.27	0.08	0.18
69	0.0	0.02	0.08	0.18	0.12	0.22	0.03	0.09
70	0.02	0.04	0.12	0.24	0.23	0.20	0.06	0.10
71	0.06	0.10	0.07	0.16	0.00	0.04	0.32	0.11

Table S1. Absolute correlations of the hinge- $\beta\beta$  residues to the latch obtained from the various MD and REMD simulations. Correlations from MD trajectories are calculated after concatenating all independent trajectories for each case into a single trajectory. The reported values correspond to the average correlation of each residue to the latch residues (residues 1-12).

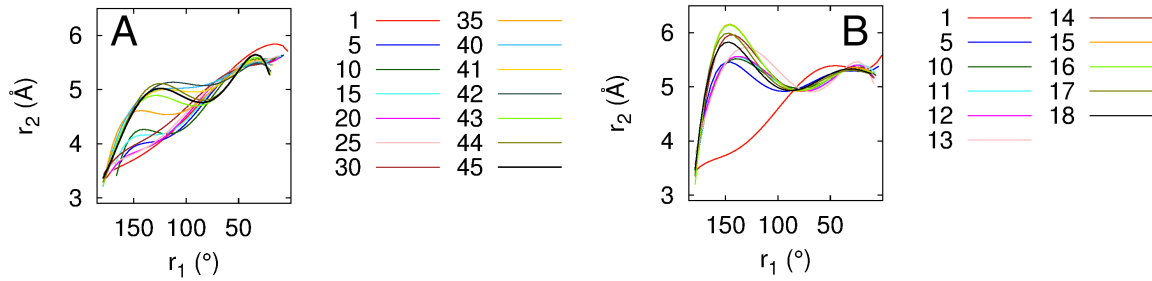


Figure S8. Convergence of the string simulations. Strings from various iterations of the simulations of VVD in DS (A) and LS (B) are plotted in the 2D space of the reaction coordinates  $r_1$  and  $r_2$  defined in Figure 5 of the main paper; iterations are color coded. During the final stages there are only small string displacements between consecutive iterations suggesting that the string has converged in the 2D space. For DS (A), the string was updated after 100 ps of MD on each image and was considered converged after 40 iterations. For LS (B), the string was updated after 500 ps of MD on each image and was considered converged after 18 iterations.

## Flavin force field parameters used in the study

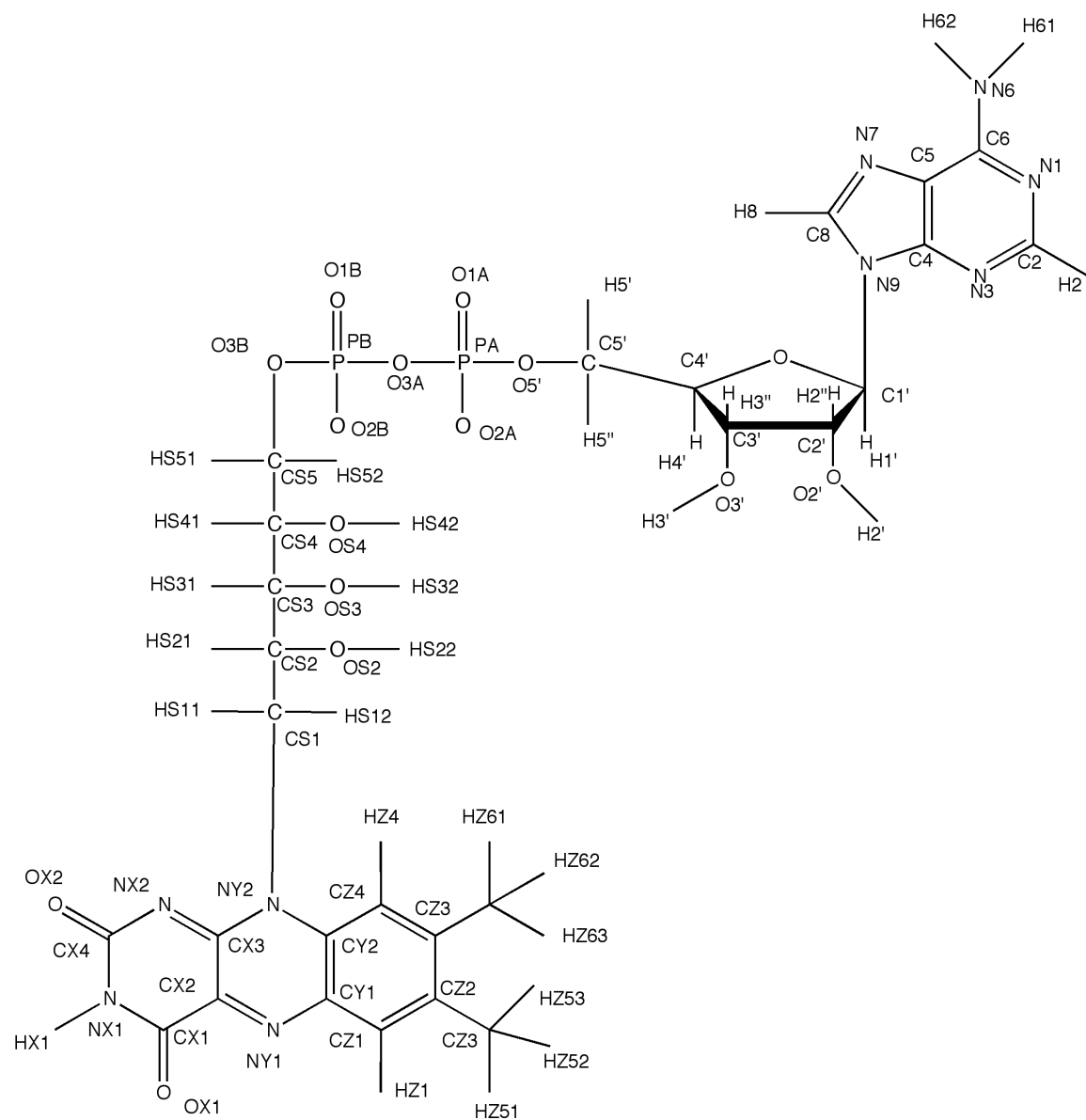


Figure S9. Chemdraw figure of flavin with atom names for reference

## Flavin in neutral semiquinone state

ATOM C4'	CN7	0.16
ATOM H4'	HN7	0.09
ATOM O4'	ON6B	-0.50
ATOM C1'	CN7B	0.16
ATOM H1'	HN7	0.09
ATOM C5	CN5	0.28
ATOM N7	NN4	-0.71
ATOM C8	CN4	0.34
ATOM H8	HN3	0.12
ATOM N9	NN2	-0.05
ATOM N1	NN3A	-0.74
ATOM C2	CN4	0.50
ATOM H2	HN3	0.13
ATOM N3	NN3A	-0.75
ATOM C4	CN5	0.43
ATOM C6	CN2	0.46
ATOM N6	NN1	-0.77
ATOM H61	HN1	0.38
ATOM H62	HN1	0.38
ATOM C2'	CN7	0.14
ATOM H2"	HN7	0.09
ATOM O2'	ON5	-0.66
ATOM H2'	HN5	0.43
ATOM C3'	CN7	0.14
ATOM H3'	HN7	0.09
ATOM O3'	ON5	-0.66
ATOM H3T	HN5	0.43
ATOM C5'	CN8	-0.08
ATOM H5'	HN8	0.09
ATOM H5"	HN8	0.09
ATOM O5'	ON2	-0.62
ATOM PA	P	1.50
ATOM O1A	ON3	-0.82
ATOM O2A	ON3	-0.82
ATOM O3A	ON2	-0.74
ATOM PB	P	1.50
ATOM O1B	ON3	-0.90
ATOM O2B	ON3	-0.90
ATOM O3B	ON2	-0.74
ATOM CS1	CT2	0.21
ATOM HS11	HA	0.09
ATOM HS12	HA	0.09
ATOM CS2	CT1	0.17
ATOM HS21	HA	0.09

ATOM OS2 OH1	-0.66
ATOM HS22 H	0.43
ATOM CS3 CT1	0.17
ATOM HS31 HA	0.09
ATOM OS3 OH1	-0.66
ATOM HS32 H	0.43
ATOM CS4 CT1	0.17
ATOM HS41 HA	0.09
ATOM OS4 OH1	-0.66
ATOM HS42 H	0.43
ATOM CS5 CT2	0.22
ATOM HS51 HA	0.09
ATOM HS52 HA	0.09
ATOM NX1 NX1	-0.89
ATOM HX1 HX1	0.43
ATOM CX1 CX1	0.82
ATOM OX1 OX1	-0.61
ATOM CX2 CX2	0.24
ATOM CX3 CX3	0.37
ATOM NX2 NX2	-0.81
ATOM CX4 CX4	1.09
ATOM OX2 OX2	-0.66
ATOM NY1 NY1	-0.60
ATOM CY1 CY1	0.60
ATOM CY2 CY2	-0.30
ATOM NY2 NY2	0.20
ATOM CZ1 CZ1	-0.46
ATOM HZ1 HZ1	0.24
ATOM CZ2 CZ2	0.19
ATOM CZ5 CT3	-0.44
ATOM HZ51 HA	0.09
ATOM HZ52 HA	0.09
ATOM HZ53 HA	0.09
ATOM CZ3 CZ3	0.18
ATOM CZ6 CT3	-0.48
ATOM HZ61 HA	0.09
ATOM HZ62 HA	0.09
ATOM HZ63 HA	0.09
ATOM CZ4 CZ4	-0.28
ATOM HZ4 HZ4	0.19

### Cysteinyl flavin adduct

ATOM C	C	0.51
ATOM O	O	-0.51
ATOM N	NH1	-0.47
ATOM HN	H	0.31
ATOM CA	CT1	0.07
ATOM HA	HB	0.09
ATOM CB	CT2	-0.181
ATOM HB1	HA	0.115
ATOM HB2	HA	0.115
ATOM SG	S	-0.141
ATOM C4'	CN7	0.16
ATOM H4'	HN7	0.09
ATOM O4'	ON6B	-0.50
ATOM C1'	CN7B	0.16
ATOM H1'	HN7	0.09
ATOM C5	CN5	0.28
ATOM N7	NN4	-0.71
ATOM C8	CN4	0.34
ATOM H8	HN3	0.12
ATOM N9	NN2	-0.05
ATOM N1	NN3A	-0.74
ATOM C2	CN4	0.50
ATOM H2	HN3	0.13
ATOM N3	NN3A	-0.75
ATOM C4	CN5	0.43
ATOM C6	CN2	0.46
ATOM N6	NN1	-0.77
ATOM H61	HN1	0.38
ATOM H62	HN1	0.38
ATOM C2'	CN7	0.14
ATOM H2"	HN7	0.09
ATOM O2'	ON5	-0.66
ATOM H2'	HN5	0.43
ATOM C3'	CN7	0.14
ATOM H3'	HN7	0.09
ATOM O3'	ON5	-0.66
ATOM H3T	HN5	0.43
ATOM C5'	CN8	-0.08
ATOM H5'	HN8	0.09
ATOM H5"	HN8	0.09
ATOM O5'	ON2	-0.62
ATOM PA	P	1.50
ATOM O1A	ON3	-0.82
ATOM O2A	ON3	-0.82

ATOM O3A ON2 -0.74  
ATOM PB P 1.50  
ATOM O1B ON3 -0.90  
ATOM O2B ON3 -0.90  
ATOM O3B ON2 -0.74  
ATOM CS1 CT2 0.012  
ATOM HS11 HA 0.078  
ATOM HS12 HA 0.078  
ATOM CS2 CT1 0.17  
ATOM HS21 HA 0.09  
ATOM OS2 OH1 -0.66  
ATOM HS22 H 0.43  
ATOM CS3 CT1 0.17  
ATOM HS31 HA 0.09  
ATOM OS3 OH1 -0.66  
ATOM HS32 H 0.43  
ATOM CS4 CT1 0.17  
ATOM HS41 HA 0.09  
ATOM OS4 OH1 -0.66  
ATOM HS42 H 0.43  
ATOM CS5 CT2 0.22  
ATOM HS51 HA 0.09  
ATOM HS52 HA 0.09  
ATOM NX1 NX1 -0.457  
ATOM HX1 HX1 0.323  
ATOM CX1 CX1 0.496  
ATOM OX1 OX1 -0.478  
ATOM CXA CXA -0.082  
ATOM CX3 CX3 0.586  
ATOM NX2 NX2 -0.654  
ATOM CX4 CX4 0.790  
ATOM OX2 OX2 -0.574  
ATOM NY1 NY1 -0.436  
ATOM HY1 HY1 0.355  
ATOM CY1 CY1 0.075  
ATOM CY2 CY2 0.054  
ATOM NY2 NY2 -0.110  
ATOM CZ1 CZ1 -0.291  
ATOM HZ1 HZ1 0.191  
ATOM CZ2 CZ2 0.078  
ATOM CZ5 CT3 -0.218  
ATOM HZ51 HA 0.077  
ATOM HZ52 HA 0.077  
ATOM HZ53 HA 0.077  
ATOM CZ3 CZ3 0.098  
ATOM CZ6 CT3 -0.254

ATOM HZ61 HA	0.083
ATOM HZ62 HA	0.083
ATOM HZ63 HA	0.083
ATOM CZ4 CZ4	-0.249
ATOM HZ4 HZ4	0.150

### Flavin in neutral semiquinone radical state

ATOM C4' CN7	0.16
ATOM H4' HN7	0.09
ATOM O4' ON6B	-0.50
ATOM C1' CN7B	0.16
ATOM H1' HN7	0.09
ATOM C5 CN5	0.28
ATOM N7 NN4	-0.71
ATOM C8 CN4	0.34
ATOM H8 HN3	0.12
ATOM N9 NN2	-0.05
ATOM N1 NN3A	-0.74
ATOM C2 CN4	0.50
ATOM H2 HN3	0.13
ATOM N3 NN3A	-0.75
ATOM C4 CN5	0.43
ATOM C6 CN2	0.46
ATOM N6 NN1	-0.77
ATOM H61 HN1	0.38
ATOM H62 HN1	0.38
ATOM C2' CN7	0.14
ATOM H2'' HN7	0.09
ATOM O2' ON5	-0.66
ATOM H2' HN5	0.43
ATOM C3' CN7	0.14
ATOM H3' HN7	0.09
ATOM O3' ON5	-0.66
ATOM H3T HN5	0.43
ATOM C5' CN8	-0.08
ATOM H5' HN8	0.09
ATOM H5'' HN8	0.09
ATOM O5' ON2	-0.62
ATOM PA P	1.50
ATOM O1A ON3	-0.82
ATOM O2A ON3	-0.82
ATOM O3A ON2	-0.74
ATOM PB P	1.50
ATOM O1B ON3	-0.90

ATOM O2B	ON3	-0.90
ATOM O3B	ON2	-0.74
ATOM CS1	CT2	-0.056
ATOM HS11	HA	0.070
ATOM HS12	HA	0.070
ATOM CS2	CT1	0.17
ATOM HS21	HA	0.09
ATOM OS2	OH1	-0.66
ATOM HS22	H	0.43
ATOM CS3	CT1	0.17
ATOM HS31	HA	0.09
ATOM OS3	OH1	-0.66
ATOM HS32	H	0.43
ATOM CS4	CT1	0.17
ATOM HS41	HA	0.09
ATOM OS4	OH1	-0.66
ATOM HS42	H	0.43
ATOM CS5	CT2	0.22
ATOM HS51	HA	0.09
ATOM HS52	HA	0.09
ATOM NX1	NX1	-0.400
ATOM HX1	HX1	0.310
ATOM CX1	CX1	0.442
ATOM OX1	OX1	-0.533
ATOM CX2	CX2	0.046
ATOM CX3	CX3	0.360
ATOM NX2	NX2	-0.590
ATOM CX4	CX4	0.717
ATOM OX2	OX2	-0.584
ATOM NY1	NY1	-0.253
ATOM HY1	HX1	0.312
ATOM CY1	CY1	0.034
ATOM CY2	CY2	0.034
ATOM NY2	NY2	-0.034
ATOM CZ1	CZ1	-0.298
ATOM HZ1	HZ1	0.194
ATOM CZ2	CZ2	0.089
ATOM CZ5	CT3	-0.199
ATOM HZ51	HA	0.072
ATOM HZ52	HA	0.072
ATOM HZ53	HA	0.072
ATOM CZ3	CZ3	0.075
ATOM CZ6	CT3	-0.221
ATOM HZ61	HA	0.078
ATOM HZ62	HA	0.078
ATOM HZ63	HA	0.078

ATOM CZ4 CZ4 -0.251  
ATOM HZ4 HZ4 0.166

Bonded parameters

CX4	NX2	350.000	1.3700
CX4	NX1	350.000	1.4000
CX4	OX2	640.000	1.1900
NX2	CX3	350.000	1.2900
CX3	CX2	282.000	1.4700
CX3	CXA	282.000	1.5200
CX2	CX1	282.000	1.5000
CXA	CX1	282.000	1.5200
CX3	NY2	350.000	1.3600
CX2	NY1	350.000	1.2700
CXA	NY1	350.000	1.4300
CX1	OX1	640.000	1.1900
CX1	NX1	350.000	1.3600
NX1	HX1	465.600	1.0000
NY2	CT2	310.000	1.4600
NY2	CY2	390.000	1.3900
CY2	CZ4	440.000	1.4000
CY2	CY1	440.000	1.4000
CY1	NY1	390.000	1.3700
CY1	CZ1	440.000	1.4000
CZ4	HZ4	370.000	1.0700
CZ4	CZ3	440.000	1.3800
CZ3	CZ2	440.000	1.4100
CZ2	CZ1	440.000	1.3700
CZ1	HZ1	370.000	1.0700
CZ2	CT3	345.000	1.5100
CZ3	CT3	345.000	1.5100
CT2	ON2	340.000	1.4400
NX2	HX2	465.600	1.0000
NY1	HY1	465.600	1.0000
NY1	HX1	465.600	1.0000
S	CXA	214.000	1.880

OX2	CX4	NX1	98.00	118.6
OX2	CX4	NX2	98.00	123.1
NX1	CX4	NX2	70.00	118.3
CX3	NX2	CX4	60.00	120.5
NX2	CX3	CX2	65.00	124.1
NX2	CX3	CXA	65.00	124.1
NX2	CX3	NY2	90.00	120.1

CX2	CX3	NY2	65.00	115.8
CXA	CX3	NY2	65.00	115.8
CX1	CX2	CX3	65.00	116.8
CX1	CXA	CX3	65.00	111.0
CX1	CX2	NY1	65.00	119.1
CX1	CXA	NY1	65.00	108.0
CX3	CX2	NY1	65.00	124.1
CX3	CXA	NY1	65.00	109.0
CX2	CX1	OX1	80.00	124.0
CXA	CX1	OX1	80.00	121.0
CX2	CX1	NX1	65.00	112.9
CXA	CX1	NX1	65.00	112.9
NX1	CX1	OX1	98.00	123.2
CX1	NX1	HX1	18.00	117.0
CX4	NX1	CX1	60.00	127.4
CX4	NX1	HX1	18.00	117.0
CX3	NY2	CT2	44.00	119.5
CT2	NY2	CY2	80.00	119.6
CX3	NY2	CY2	60.00	120.9
NY2	CY2	CZ4	65.00	122.7
NY2	CY2	CY1	65.00	118.9
CZ4	CY2	CY1	70.00	118.4
CY2	CY1	NY1	65.00	121.2
CY2	CY1	CZ1	70.00	120.1
NY1	CY1	CZ1	65.00	118.7
CY1	NY1	CX2	60.00	119.2
CY1	NY1	CXA	60.00	119.2
CY2	CZ4	HZ4	31.00	120.2
CZ3	CZ4	HZ4	31.00	118.6
CY2	CZ4	CZ3	70.00	121.1
CZ4	CZ3	CZ2	70.00	120.5
CZ4	CZ3	CT3	70.00	119.3
CZ2	CZ3	CT3	70.00	120.2
CZ1	CZ2	CZ3	70.00	118.1
CZ3	CZ2	CT3	70.00	121.2
CZ1	CZ2	CT3	70.00	120.7
CZ2	CZ1	CY1	70.00	121.8
CZ2	CZ1	HZ1	31.00	121.2
CY1	CZ1	HZ1	31.00	117.1
CZ2	CT3	HA	35.00	115.0
CZ3	CT3	HA	35.00	115.0
NY2	CT2	HA	46.50	106.2
NY2	CT2	CT1	65.00	109.5
CN8	CN7	ON6B	110.00	109.0
ON6B	CN7B	CN7	110.00	105.0
NN2	CN7B	CN7	70.00	113.7

CN7	CN7	CN7		53.35	111.0	8.0	2.561
CN7	CN8	ON2		75.70	110.1		
P	ON2	CT2		20.0	120.0	35.	2.33
CT2	CT1	OH1		75.700	110.10		
ON2	CT2	CT1		75.700	110.10		
ON2	CT2	HA		45.900	108.89		
CX3	NX2	HX2		18.00	117.0		
CX4	NX2	HX2		18.00	117.0		
CZ3	CT3	S		35.00	115.0		
CX1	CXA	S		35.00	103.0		
CX3	CXA	S		35.00	111.0		
NY1	CXA	S		35.00	115.0		
HY1	NY1	CY1		35.00	116.0		
HX1	NY1	CX2		35.00	116.0		
HX1	NY1	CY1		35.00	116.0		
HY1	NY1	CXA		35.00	113.0		
HX1	NY1	CXA		35.00	113.0		
CT2	S	CXA		35.00	107.0		

ON3	P	ON2	CT2	0.10	3	0.0	
X	CX4	NX2	X	2.05	2	180.0	
X	NX2	CX3	X	2.05	2	180.0	
X	CX2	CX3	X	0.50	2	180.0	
X	CXA	CX3	X	0.50	2	180.0	
X	CX1	CX2	X	0.50	2	180.0	
X	CX1	CXA	X	0.50	2	180.0	
X	CX1	NX1	X	2.05	2	180.0	
X	CX4	NX1	X	2.05	2	180.0	
X	CX3	NY2	X	2.05	2	180.0	
X	CY2	NY2	X	2.05	2	180.0	
X	CY1	CY2	X	3.10	2	180.0	
X	NY1	CY1	X	2.05	2	180.0	
X	NY1	CX2	X	2.05	2	180.0	
X	NY1	CXA	X	2.05	2	180.0	
X	CY2	CZ4	X	3.10	2	180.0	
X	CZ4	CZ3	X	3.10	2	180.0	
X	CZ2	CZ3	X	3.10	2	180.0	
X	CZ1	CZ2	X	3.10	2	180.0	
X	CY1	CZ1	X	3.10	2	180.0	
X	CZ2	CT3	X	0.10	3	0.0	
X	CZ3	CT3	X	0.10	3	0.0	
X	CT2	NY2	X	0.01	3	0.0	
X	CN7	CN7	X	0.15	3	0.0	
X	CT2	ON2	X	0.25	3	0.0	
X	ON6B	CN7B	X	0.10	3	0.0	

X	CN7	CN8	X	0.200	3	0.0
X	CN7	CN7B	X	0.15	3	0.0
X	CN7	ON6B	X	0.10	3	0.0
X	CN8	ON2	X	-0.10	3	0.0
ON2	P	ON2	CT2	0.95	2	0.0
X	CX3	NX2	X	2.05	2	180.0
X	CX4	NX2	X	2.05	2	180.0
CT3	S	CT2	CT1	0.2400	1	0.00
CT3	S	CT2	CT1	0.1500	2	0.00
CT3	S	CT2	CT1	0.2700	3	0.00
CZ3	CT3	S	CT2	0.2800	3	0.00
CXA	S	CT2	CT1	0.1000	3	0.00
X	S	CXA	X	0.1000	3	0.00
HA	CT2	S	CXA	0.1000	3	0.00

#### Non bonded parameters

CX1	0.000000	-0.141000	1.870000
CX2	0.000000	-0.141000	1.870000
CXA	0.000000	-0.141000	1.870000
CX3	0.000000	-0.141000	1.870000
CX4	0.000000	-0.141000	1.870000
CY1	0.000000	-0.141000	1.870000
CY2	0.000000	-0.141000	1.870000
CZ1	0.000000	-0.141000	1.870000
CZ2	0.000000	-0.141000	1.870000
CZ3	0.000000	-0.141000	1.870000
CZ4	0.000000	-0.141000	1.870000
HX1	0.000000	-0.049800	0.800000
HZ1	0.000000	-0.042000	1.330000
HZ4	0.000000	-0.042000	1.330000
NX1	0.000000	-0.090000	1.830000
NX2	0.000000	-0.090000	1.830000
NY1	0.000000	-0.090000	1.830000
NY2	0.000000	-0.090000	1.830000
OX1	0.000000	-0.120000	1.700000
OX2	0.000000	-0.120000	1.700000
HX2	0.000000	-0.049800	0.800000
HY1	0.000000	-0.049800	0.800000